


Shear rheology of polylactide (PLA)–cellulose nanocrystal (CNC) nanocomposites

Davood Bagheriasl · Pierre J. Carreau  · Bernard Riedl · Charles Dubois · Wadood Y. Hamad

Received: 13 November 2015 / Accepted: 18 March 2016 / Published online: 21 March 2016
© Springer Science+Business Media Dordrecht 2016

Abstract A simple method for the preparation of polymer-cellulose nanocrystal (CNC) nanocomposite is shown to yield good dispersion of CNCs within a polylactide (PLA) matrix, which consequently resulted in the lowest rheological percolation threshold reported so far for polymer-CNC systems. The rheological behavior of the nanocomposites was determined in dynamic, transient, and steady-shear flow fields in the molten state. The complex viscosity and storage modulus of the nanocomposites increased markedly with CNC content, particularly at low frequencies; the samples were highly shear thinning and exhibited a transition from liquid- to solid-like behavior as the CNC concentration increased. Larger values for steady-state viscosity, yield stress, shear stress, and first normal stress difference were reported

for the more concentrated nanocomposites. Also, pronounced overshoots in the transient start-up viscosity of the nanocomposites were observed. These results could be ascribed to the formation of an interconnected CNC network within the PLA matrix.

Keywords Nanocomposites · Cellulose nanocrystals (CNCs) · Polylactide · Rheological properties · Dispersion

Introduction

Cellulose is the most common biomacromolecule on earth and constitutes the structural matter of all plants. Therefore, there have always been searches for new applications of cellulose due to the low cost, abundance in nature, renewability, and biodegradability. Cellulose and its derivatives in different forms have been used for energy source, paper, building material, clothing, foodstuffs, pharmaceuticals, films, coatings, and membranes for many years (Klemm et al. 2005, 2011). One form of cellulose that has attracted interest and importance is nano cellulose, especially cellulose nanocrystal (CNC). CNCs are rodlike particles with nanoscale dimensions and provide several interesting properties such as biodegradability, low density, abundance in nature, very large surface area, and high strength, which can be of interest for many applications (Klemm et al. 2011). Over the last years, the

D. Bagheriasl · P. J. Carreau (✉) · C. Dubois
Research Center for High Performance Polymer
and Composite Systems (CREPEC), Chemical
Engineering Department, Polytechnique Montreal,
PO Box 6079, Stn Centre-Ville, Montreal, QC H3C 3A7,
Canada
e-mail: pcarreau@polymtl.ca

B. Riedl
Département des sciences du bois et de la forêt, Faculté de
foresterie, géographie et géomatique, Université Laval,
Quebec, QC G1V 0A6, Canada

W. Y. Hamad
FPInnovations, 2665 East Mall, Vancouver, BC V6T 1Z4,
Canada

combination of these properties has made CNC an interesting reinforcing agent in polymer composite industry. However, some of their features such as strong inter-particle interactions due to hydrogen bonds make it difficult to obtain a good dispersion and, consequently, enhanced properties when incorporated in hydrophobic polymers. That is why obtaining a good dispersion of CNCs in hydrophobic polymers remains a challenge, in particular without the use of any compatibilizer or CNC modification. The first use of CNCs as a reinforcing agent in polymers was reported by Favier et al. (1995) who could enhance the mechanical properties of solution-cast films of poly(styrene-co-butyl acrylate) latex. Since then, their applications as reinforcing agents in polymers have grown, but limited to a few hydrophilic polymers or polymers in latex form (Abitbol et al. 2011; Bendahou et al. 2010; Favier et al. 1995; Park et al. 2007; Peresin et al. 2010; Siqueira et al. 2010; Zhang et al. 2014). CNC surface modification or compatibilization was necessary to achieve a good CNC dispersion in most of common polymers (Bagheriasl et al. 2015; Goffin et al. 2011a, b; Morandi et al. 2009; Raquez et al. 2012; Siqueira et al. 2009, 2013).

Recently, there has been increasing interest to incorporate CNCs into biopolymers to expand their applications by improving their properties. Such combinations of biorenewable, biocompatible, and biodegradable components would create a new category in composite materials that can replace petroleum-based polymeric products, especially in packaging and automotive industries. However, obtaining a fairly good dispersion of CNCs within the chosen matrix is necessary in order to achieve enhanced properties for the resulting biocomposites at low nanoparticle concentrations. Among the numerous investigations conducted to achieve fairly good dispersion of CNCs only a few considered the rheological characterization of polymer-CNC systems (Arias et al. 2015; Bitinis et al. 2013; Goffin et al. 2011b; Kamal and Khoshkava 2015; Khoshkava and Kamal 2014; Mabrouk et al. 2011; Pereda et al. 2014). The formation of an interconnect network of particles plays an important role on the rheological properties of a nanocomposite system. Therefore, the rheological behavior of the resulting nanocomposites can reveal whether the preparation method is efficient in leading to nano dispersions. Pereda et al. (2014) reported

reduced viscosity values for 1 wt% polyethylene oxide (PEO) aqueous solutions with different CNC loadings in steady-shear flow experiments for a wide range of shear rates. Arias et al. (2015) could obtain a good dispersion of CNCs in a polylactide (PLA) of a low molecular weight via a PEO-CNC masterbatch preparation. However, the complex viscosity of the resulting nanocomposites did not show any changes compared to those of the neat PLA and PLA filled with CNCs in absence of PEO. The rheological behavior in small-amplitude oscillatory shear (SAOS) and steady-shear flows of polypropylene (PP)-CNC nanocomposites was investigated by Khoshkava and Kamal (2014). They determined the effects of the CNC drying process, initial concentration of the CNC aqueous suspensions and final concentration in the nanocomposites on the properties of PP-CNC systems. A value of 2.5 wt% was reported as the rheological percolation threshold in the best case, where the initial concentration of CNCs in the aqueous suspension was 1 wt% and the CNCs were spray-freeze dried (Khoshkava and Kamal 2014). Kamal and Khoshkava (2015) used the same method to prepare PLA-CNC nanocomposites and reported significant increases of the complex viscosity, storage and loss moduli for the PLA filled with spray-freeze dried CNCs compared to the neat PLA. An increased storage modulus in SAOS experiments for a polycaprolactone (PCL) filled with PCL-grafted CNCs was reported by Goffin et al. (2011b); the increase was attributed to a better state of dispersion of the CNCs in PCL, obtained by in situ ring-opening polymerization of the lactone in presence of the CNCs. Mabrouk et al. (2011) reported increases of the complex viscosity and storage modulus at low frequencies, up to almost 4 and 5 orders of magnitude, respectively, for nanocomposites based on a poly(styrene-co-hexylacrylate) copolymer and cellulose whiskers prepared via in situ polymerization of styrene and 2-ethylhexylacrylate. Increased complex viscosity and storage modulus for blends of PLA and natural rubber (NR) filled with unmodified CNCs and CNCs grafted with C₁₈ alkyl chains were reported by Bitinis et al. (2013). However, their results did not show significant changes for PLA-NR blends filled with PLA grafted CNCs.

In this work the effect of the CNCs on the rheological properties of polylactide was investigated. To this end, a solution casting method with a polar solvent was used to favor a better dispersion of

hydrophilic CNCs within a PLA matrix without the need of CNC modification or use of any compatibilizer. To stress the efficiency of the solvent mixing method, the rheological properties of samples of PLA–CNC at a CNC content of 2 wt% prepared via direct melt mixing and the solution casting method are compared. Our objective is first to develop biobased and biodegradable PLA–CNC nanocomposites with a dispersed structure via a simple method and, second, to characterize the rheological behavior of these nanocomposites for different shear flow fields. To our knowledge, this is the first time that the rheological behavior of polymer–CNC nanocomposites in different shear flow fields is systematically reported.

Experimental section

Materials

A commercial grade polylactide (PLA) (Ingeo Biopolymer 3251D) with MFR of 35 g/10 min (190 °C/2.16 kg), crystalline melting temperature of 155–170 °C and glass transition temperature (T_g) of 55–60 °C was purchased from NatureWorks LLC (Minnetonka, MN, USA) and used as the matrix. N,N-dimethylformamide (DMF), anhydrous 99.8 %, was purchased from Sigma-Aldrich Canada Co. (Oakville, ON, Canada). Freeze-dried CNCs were kindly provided by FPIInnovations (Pointe-Claire, QC, Canada). The details of CNC preparation is provided elsewhere (Hamad and Hu 2010).

Sample preparation

To prepare the nanocomposites a solution mixing method in DMF medium was used. The desired amount of CNCs were first dispersed in 135 mL of DMF using a water-bath sonicator (FS30 100 Watts Ultrasonic Cleaner, Fisher Scientific, Pittsburg, PA) during 2 h; then, 40 g of PLA was added and the mixture was heated up to ca. 70 °C while stirring during 150 min with a magnetic stirrer until the complete dissolution of the PLA. The mixture was finally poured on a tray and dried in a vacuum oven at 80 °C for 36 h. Using a coffee grinder, the product was ground into powder and kept in the oven at 60 °C for another 36 h. For the sake of comparison, PLA–CNC composite samples were also prepared via melt

mixing: the CNCs and PLA were introduced in an internal mixer, DDRV501 Brabender (C. W. Brabender Instruments Inc., NJ, USA), and melt-compounded at 180 °C, 100 rpm for 7 min under N₂ atmosphere. Thereafter, all samples were compression molded for 10 min at 175 °C in the presence of N₂ followed by 5 min at room temperature to prepare the test specimens. The nanocomposites were coded according to their CNC content on a weight percentage basis. For instance, PLA4CNC denotes the nanocomposite containing 4 wt% CNCs, based on total weight of the nanocomposite.

Characterization

Microscopy

Transmission electron microscopy (TEM) analysis was conducted on ultra-microtomed samples using a JEOL JEM-2100F microscope (JEOL USA Inc., Peabody, MA, USA), operating at 200 kV. The samples were microtomed into slices with an approximately 50–80 nm thickness at ca. –100 °C using an Ultracut FC microtome (LEICA) with a diamond knife. For a better visualization the samples were stained using a bis(ethylenediamine)copper(II) hydroxide solution (copper(II)-ethylenediamine complex) 1.0 M in H₂O purchased from Sigma-Aldrich Canada Co. (Oakville, ON, Canada). To this end, first, the copper(II)-ethylenediamine complex was diluted to 1 wt% solution with deionized (DI) water; then, the ultra-microtomed samples placed on copper grids were immersed in the solution for 150 s. To remove the excess of the absorbed solution the samples were successively immersed in DI water three times, each time in fresh water for 10 s. Finally, the samples were left at room temperature for 24 h to avoid fracture of the stained layer due to fast evaporation, followed by another 24 h in a desiccator before TEM analysis.

Scanning electron microscopy (SEM) analysis was carried out on ultra-microtomed surfaces, coated with gold. The microscope was a JEOL JSM 7600TFE scanning electron microscope (SEM) (JEOL USA Inc., Peabody, MA, USA) operated at 2 kV.

Rheology

The rheological properties of the neat PLA and the nanocomposites were measured using a stress-

controlled MCR 301 rheometer (Anton Paar, Austria). The experiments were conducted under a nitrogen atmosphere to avoid oxidation of the samples. A cone-and-plate geometry was used with a truncation of 51 μm , cone angle of 1.98° , parallelity of $\pm 1 \mu\text{m}$ and a diameter of 25 mm. Time-sweep experiments at strain amplitude of 0.05 and frequency of 1 rad s^{-1} were conducted to verify the thermal stability of samples within the time required to do small-amplitude oscillatory shear (SAOS) experiments. SAOS tests were performed at strain amplitude of 0.05 to ensure the measurements were in the linear viscoelastic regime. Steady-shear experiments were also performed over a wide range of shear rate and shear stress-growth experiments were conducted at a rate of 5 s^{-1} in forward and reverse directions for different rest times between consecutive tests, 0, 200 and 1000 s. Finally, time-sweep tests at strain amplitude of 0.05 and frequency of 1 rad s^{-1} were performed right after the stress-growth tests to monitor the structure build-up in samples. All the rheological measurements were performed at 170°C .

Results and discussion

Microscopy

Figure 1 depicts a TEM image of CNCs, and SEM and TEM images of PLA containing 4 wt% CNC (PLA4CNC). The TEM image in Fig. 1a was obtained for an aqueous suspension containing 0.5 wt% CNCs. It shows individual and bundles of few CNCs; from over 200 measurements via the ImageJ software, the average particle width, length, and aspect ratio were found to be 16 ± 3 , $90 \pm 17 \text{ nm}$ and 6 ± 2 , respectively. Figure 1b presents a SEM image of PLA4CNC (nanocomposite containing 4 wt% CNCs); some agglomerates of CNCs are obviously formed within the PLA and those are fibrillar and of random-shaped size in the range of 1–3 μm . Individual CNCs and bundles of few individual CNCs dispersed into the PLA matrix are observed in the TEM images of Fig. 1c, d for two different locations. The nanoparticles seem to have the same dimension size as observed in Fig. 1a. These images reveal that the solution preparation method used could lead to a good dispersion of the CNCs, down to the individual size or bundles of few individual CNCs. In fact, initially the

CNCs were well dispersed in DMF by means of the sonicator and, then, when the PLA was added and dissolved the individual nanoparticles could be trapped within the PLA chains and this structure remains after solvent casting. The TEM images of Fig. 1c, d validate our assumption that the solution preparation method is efficient in dispersing the CNCs into the PLA, although some small agglomerates in the range of few (1–3) μm are observed (Fig. 1b).

Rheology

SAOS

All samples exhibited stable rheological properties, with changes of less than 2 %, in time-sweep experiments over 15 min. Figure 2 presents the complex viscosity, η^* , and storage modulus, G' , versus frequency, ω , of the neat PLA and PLA–CNC nanocomposites with CNC loadings varying from 1 to 7 wt%. In oscillatory shear η^* is the ratio of the shear stress amplitude to the strain rate amplitude, which are not in phase for viscoelastic fluids and can be written as real and imaginary parts (Carreau et al. 1997); G' is related to the imaginary part of the complex viscosity and is a measure of the energy stored in the material during half a cycle. The complex viscosity, η^* , of the neat PLA exhibits a long plateau, with a slight shear-thinning behavior at high frequencies (Fig. 2a) and its storage modulus, G' , is typical of molten polymers with a terminal zone of slope equal to 2 on the log–log plot of G' versus ω (Fig. 2b). For all nanocomposites, even those with CNC concentration as low as 0.5 wt%, spectacular increases of η^* and G' are observed, mainly at low frequencies, which clearly show the strong effect of CNCs on the rheological properties of PLA. At 1 wt% CNC, η^* and G' increase by 1 and 4 orders of magnitude, respectively relative to the neat PLA (Fig. 2). Further increases in both η^* and G' , up to 3 and 6 orders of magnitude, respectively, are observed for the nanocomposite samples at larger CNC concentrations. All nanocomposite samples exhibit a shear-thinning behavior for η^* without any plateau region at low frequencies and G' that tends towards a plateau at low frequencies. We can infer that these results indicate the formation of a network and a transition from liquid- to solid-like behavior as observed for many polymer nanocomposites, attributed to the good dispersion of the CNCs in the PLA.

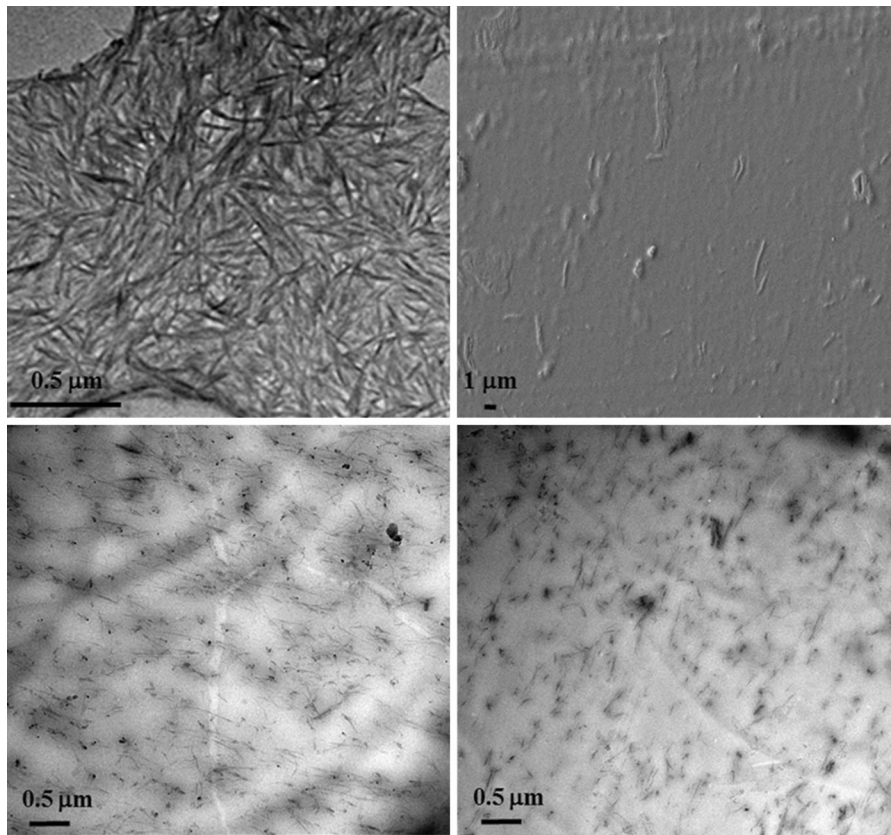


Fig. 1 TEM image of CNCs taken from an aqueous suspension of 0.5 wt% CNC (a), SEM micrograph of PLA4CNC (b), and TEM images at two different locations for PLA4CNC (c, d)

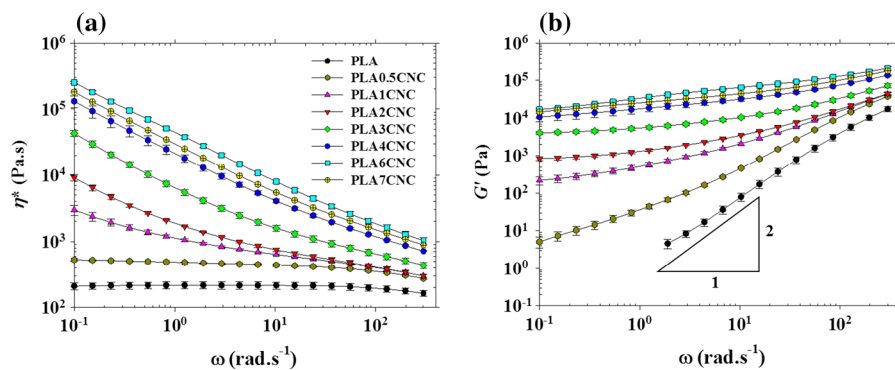


Fig. 2 Complex viscosity, η^* , (a) and storage modulus, G' , (b) versus frequency, ω , of the neat PLA and PLA–CNC nanocomposites at 170 °C (strain = 5 %)

Similar rheological behavior in SAOS has been reported for other polymer nanocomposites containing CNCs, clays or carbon nanotubes for which a good dispersion was achieved (Abbasi et al. 2009; Goffin et al. 2011b; Khoshkava and Kamal 2014; Sinha Ray

et al. 2003). It is worth mentioning that the SAOS data of PLA containing 7 wt% CNC are lower than those of the PLA filled with 6 wt%. This can be explained by a significant formation of agglomerates at this high CNC content.

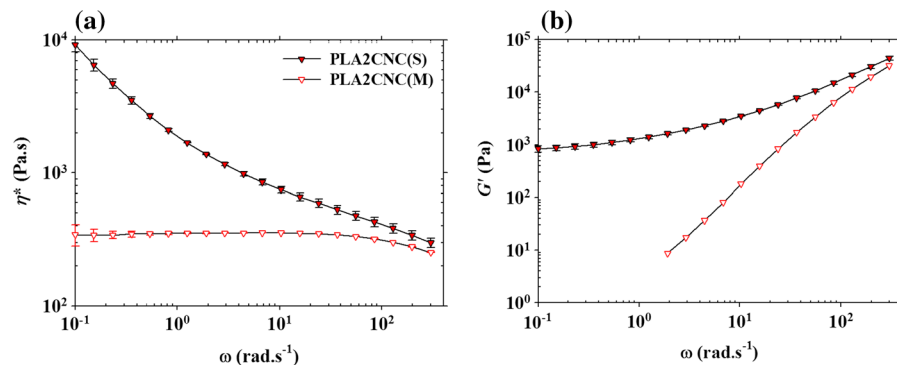


Fig. 3 Comparison of η^* (a) and G' (b) versus ω of PLA2CNC prepared via solution (S) and melt (M) method

Figure 3 compares the efficiency of the solution preparation method utilized in the present work over the melt mixing preparation. Although at high frequencies the values of η^* and G' of all samples are in the same range, huge differences in η^* and G' of the PLA containing 2 wt% CNCs prepared in solution (PLA2CNC(S)) are observed at low frequencies compared to PLA2CNC(M), prepared in melt. This comparison reveals the efficiency of the solution method for preparing PLA–CNC nanocomposites over the melt preparation approach, which does not show significant improvements in the rheological behavior compared to that of the neat PLA shown in Fig. 2. We can conclude that the novel and simple method used in this work led to a good dispersion resulting in large increases in viscosity and modulus that have never been reported for polymer–CNC systems.

It is well known that an interconnected structure of nanoparticles in a polymeric matrix can result in a solid-like behavior with an unbounded viscosity, a plateau in G' at low frequencies and an apparent yield stress. To better show the apparent yield stress we have made plots of the complex viscosity as a function of the complex modulus, G^* , in log–log scales as illustrated in Fig. 4. For the neat PLA and PLA0.5CNC samples no apparent yield stress is observed while for other nanocomposites a viscosity up-turn can be seen as G^* decreases. The apparent yield stress can be easily obtained by using a modified Herschel–Bulkley model:

$$\eta^* = \frac{G_0^*}{\omega} + k(\gamma^0 \omega)^{n-1} \quad (1)$$

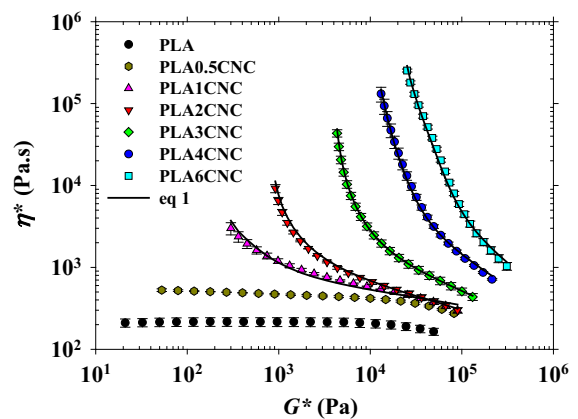


Fig. 4 Complex viscosity, η^* , versus the complex modulus, G^* , of the neat PLA and PLA–CNC nanocomposites. The lines are the fits of the modified Herschel–Bulkley model (Eq. 1)

$$\sigma_0 = G_0^* \gamma^0 \quad (2)$$

where G_0^* is the magnitude of the complex modulus at the lowest frequency, γ^0 is the strain amplitude ($=0.05$), k is a constant and n is the flow index (Ghanbari et al. 2013). The fitting parameters for the modified Herschel–Bulkley model are presented in Table 1. As expected the apparent yield stress, σ_0 , increases with CNC content while n decreases. The increasing σ_0 can be ascribed to stronger particle–particle and polymer–particle interactions, which induce more restriction to chain mobility (Ghanbari et al. 2013). For the PLA containing 6 wt% CNCs almost the same σ_0 value was obtained by Kamal and Khoshkava (2015); however, for less concentrated systems they reported much lower values compared to

Table 1 Yield stress and melt flow index of the nanocomposites using the Herschel–Bulkley model (Eq. 4) and the modified Herschel–Bulkley model (Eqs. 1, 2)

CNC content (wt%)	SAOS			Steady shear		
	σ_0 (Pa)	k (Pa s ^{<i>n</i>})	<i>n</i>	τ_0 (Pa)	a (Pa s ^{<i>n</i>})	<i>n</i>
1	15.0	505	0.86	52.7	640	0.73
2	45.9	581	0.76	107	856	0.69
3	217	966	0.70	334	1450	0.60
4	655	2040	0.62	847	2970	0.50
6	1260	3490	0.56	1280	4730	0.38

our results. Another useful information that can be obtained from Fig. 4 is the CNC concentration at which rheological percolation occurs. The PLA with 1 wt% CNC shows an apparent yield stress while this is not the case for the 0.5 wt% CNC sample. Therefore, the rheological percolation threshold should be between 0.5 and 1 wt%, as confirmed below.

Rheological percolation threshold

The rheological percolation threshold is the content of solid particle above which the rheological properties of suspension increase exponentially and exhibit an apparent yield stress. In the previous section this value was estimated to fall in the range of 0.5–1 wt% CNCs. To have a more precise value, the storage modulus of the samples at the lowest measured frequency in SAOS experiments (here 0.1 rad s⁻¹) is plotted versus the CNC content in Fig. 5. The percolation threshold can be obtained by using an empirical power-law relation defined as

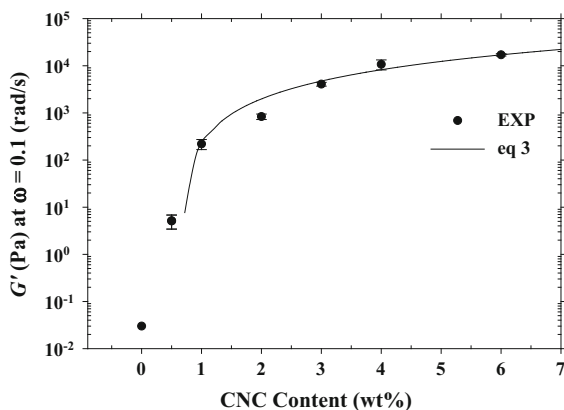


Fig. 5 Storage modulus of the PLA–CNC nanocomposites as a function of the CNC loading obtained at 170 °C and $\omega = 0.1$ rad s⁻¹. The line is a fit with the power-law expression of Eq. 3. Note that the value of the neat PLA was obtained after extrapolation to $\omega = 0.1$ rad s⁻¹

$$G' = \beta_c G \left(\frac{m - m_c G}{m_c G} \right)^n \quad \text{for } m > m_c G \quad (3)$$

where $\beta_c G$ and n are power-law constants, m is the CNC concentration (wt%) and $m_c G$ is the rheological percolation threshold (wt%) (Abbasi et al. 2009; Du et al. 2004; Hu et al. 2006). A value of 0.68 wt% is obtained from the fit of the data of Fig. 5 using Eq. 3. This is much smaller than the values of 2.5 and 3 wt% reported elsewhere for the rheological percolation threshold of PP and PLA filled CNCs, respectively (Kamal and Khoshkava 2015; Khoshkava and Kamal 2014). This again reveals that a better dispersion was achieved in the present work.

Steady-shear flow

Figure 6 presents the steady-shear viscosity, η , (ratio of shear stress to shear rate under simple steady-shear flow) over a wide range of shear rates for the neat PLA and PLA containing 1 and 4 wt% CNCs. Similar to the behavior shown previously in SAOS experiments (Fig. 2), a shear-thinning behavior without any plateau region and unbounded viscosity at low shear rates for the PLA containing 1 and 4 wt% CNC are observed while the neat PLA shows a Newtonian behavior. Figure 6a compares the shear viscosity of the samples when two consecutive tests were conducted from low-to-high shear rates (filled symbols) with that of high-to-low experiments (open symbols) using the same samples. Clearly higher viscosities for the low-to-high experiments are observed at low shear rates. In fact, when a test is performed from low-to-high shear rates the CNC network within the PLA matrix is gradually destroyed as the shear rate increases. Hence, in the second experiments conducted from high-to-low shear rates on the same sample, lower viscosity values are observed. From this thixotropic behavior of PLA filled CNC samples observed in Fig. 6a it can be concluded

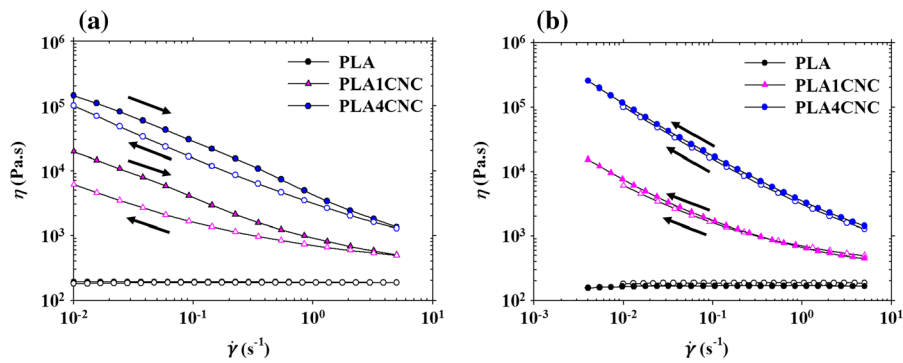


Fig. 6 Variation of the steady-state viscosity versus shear rate of the neat PLA and nanocomposite samples; **a** filled symbols represent the experiments performed from low-to-high shear rates while the open symbols show the results of measurements

from high-to-low on the same samples. **b** The two consecutive experiments were both conducted from high-to-low shear rates; open symbols: first test; filled symbols, second test

that the CNC network broken down in a low-to-high shear test cannot be reformed with the same strength in a high-to-low shear test. Figure 6b compares the viscosities of fresh samples for two consecutive high-to-low shear tests. Obviously, the data for both tests superpose indicating again that the structure broken down at high shear rates cannot be totally reformed at low shear rates.

The original Herschel–Bulkley model used to fit the steady-shear data of Fig. 7a is expressed as

$$\tau = \tau_0 + a\dot{\gamma}^n \tag{4}$$

where τ_0 is the apparent yield stress in simple shear and, n , is power-law (melt flow) index. The fitting parameters of the Herschel–Bulkley model are presented in Table 1. For the neat PLA no yield stress is observed while as CNCs are added to the PLA an apparent yield stress is observed, as reported above for

the SAOS data. We note with surprise from Table 1 that the apparent yield stress values obtained from steady-shear data are considerably larger than those obtained from SAOS data, except for PLA6CNC. This is due to the low strain amplitude used in Eq. 2 to evaluate the yield stress from SAOS tests. Obviously, the structure will breakdown at much larger strain amplitudes. Moreover, complexities associated with measuring the yield stress via extrapolation methods and using empirical equations should be considered. Figure 7b presents the first normal stress difference, N_1 , as a function of shear rate for the PLA–CNC nanocomposites. N_1 depicts a plateau at low shear rates and, then, increases with $\dot{\gamma}$ at higher rates. As expected, N_1 increases with increasing CNC concentration in the PLA and these larger normal stress differences are the sign of stronger particle–particle interactions and a more elastic network. Similar

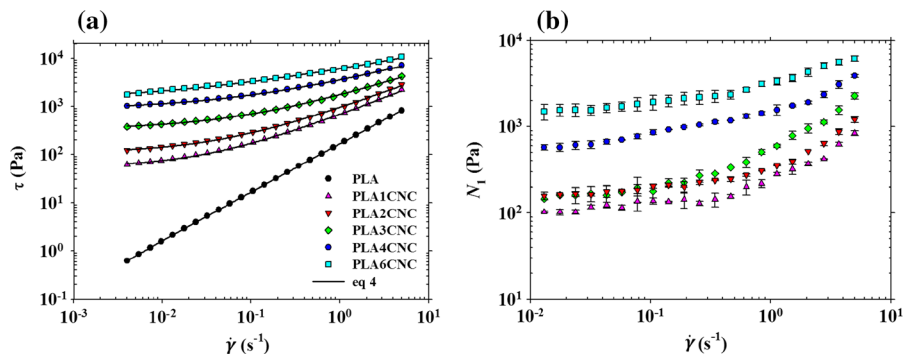


Fig. 7 Steady-state stress data for the PLA–CNC nanocomposites from high-to-low shear rate measurements; **a** shear stress versus shear rate. The lines are fits of the Herschel–Bulkley model (Eq. 4). **b** First normal stress difference versus shear rate

behavior has been reported for epoxy and carbon nanotube (CNT) systems by Natale et al. (2014). They developed a model that predicts that the contribution of the particle–particle interactions is a linear function of $\dot{\gamma}$ while that of the network elasticity decreases with shear rate due to the destruction of the network.

Cox–Merz rule

The Cox–Merz rule states that the steady-state viscosity $\eta(\dot{\gamma})$ and complex viscosity $\eta^*(\omega)$ are equal when compared at $\dot{\gamma} = \omega$ (Cox and Merz 1958; Shafiei-Sabet et al. 2012). This rule is not expected to be applicable for filled polymer systems, in particular nanocomposites. To verify this, the complex viscosity versus angular frequency in SAOS experiments is compared to the steady-shear viscosity versus shear rate in Fig. 8a. As anticipated, the neat PLA follows the Cox–Merz rule. However, the PLA–CNC nanocomposites deviate largely from this rule. For both PLA1CNC and PLA4CNC samples, larger η^* values are observed compared to the η values and the differences are much larger for PLA4CNC relative to PLA1CNC. This can be explained by the structure breakdown in steady-shear flows. In fact, this rule is obeyed by isotropic systems or systems with negligible/minimal structure (Shafiei-Sabet et al. 2012). For filled systems that show yield stress another correlation is suggested, which is referred to as the extended Cox–Merz rule (Doraiswamy et al. 1991). According to this relation, if the steady-state viscosity η and the complex viscosity η^* are plotted versus shear rate $\dot{\gamma}$ and $\gamma^0\omega$, respectively, where γ^0 is the strain amplitude of the SAOS experiments, the curves will superimpose

(Doraiswamy et al. 1991). Figure 8b compares the two curves. An acceptable agreement of this rule is observed for the neat PLA and PLA4CNC samples. However, for the PLA containing 1 wt% CNC large deviations are seen at low rates.

Transient flow

Figure 9 compares the rheological behavior of samples for start-up or stress growth experiments in forward (Fig. 9a) and reverse (Fig. 9b) flows. It should be mentioned that the error is estimated to be less than 10 %. In the filled systems the observation of an overshoot in transient viscosity, η^+ , (Sepehr et al. 2004) shear stress, σ^+ , (Letwimolnun et al. 2007), and first normal stress difference, N_1^+ , (Sepehr et al. 2004) versus time or strain can be attributed to the structure or networks of particles within the polymer matrices. Here, the variations of the transient viscosity, η^+ , with time are presented in Fig. 9a for the forward flow. As expected, the neat PLA does not show overshoot due to the absence of any structure and of its low viscoelasticity. However, for the PLA–CNC nanocomposites overshoots at the beginning of the tests, corresponding to a low deformation of about 1, are observed for all concentrations, which can be attributed to the strong CNC network within the PLA. A similar behavior for PP–CNC nanocomposites was reported in our previous work when a good dispersion of the CNCs was achieved (Bagheriasl et al. 2015). The overshoot becomes larger as the concentration of CNC increases revealing a stronger CNC network. These transient tests are destructive and the structure will be rebuilt under rest. Figure 9b depicts the

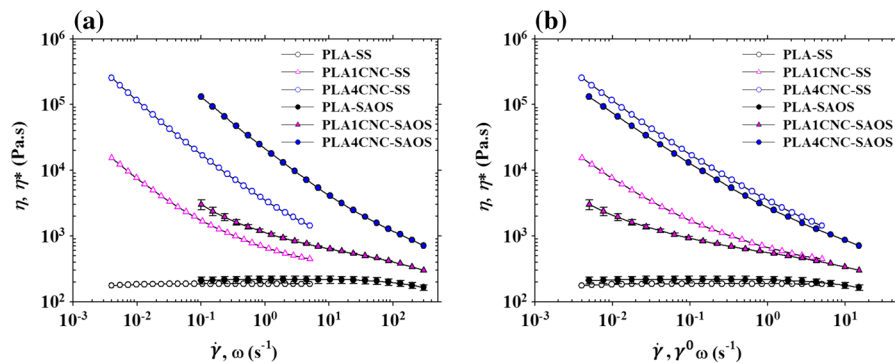
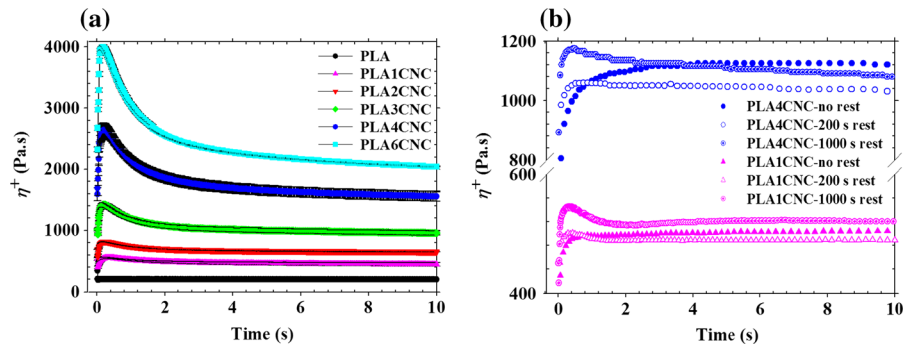


Fig. 8 Variation of the steady-state and complex viscosities of the neat PLA and nanocomposite samples versus **a** shear rate and frequency, and **b** shear rate and $\gamma^0\omega$, respectively

Fig. 9 Variations of the shear stress growth coefficient, η^+ , of the PLA and PLA–CNC nanocomposites as functions of time for an imposed shear rate $\dot{\gamma} = 5 \text{ s}^{-1}$ in forward (a) and reversed flow after 0, 200, and 1000 s (b)



behavior of the samples in the reverse flow right after, 200, and 1000 s after the first forward flow. No overshoot is observed when the reverse test is performed right after the forward flow. Small overshoots for both PLA1CNC and PLA4CNC are seen after 200 s rest time while after a longer rest time (1000 s) a larger overshoot is observed. In fact in the forward flow, the structure in the samples is broken down and the CNCs possibly orient themselves in the flow direction. When the flow is immediately reversed the nanoparticles need time to form any structure and also due to their short length they cannot tilt over as observed for fiber suspensions (Sephehr et al. 2004). However, with increasing rest time particle–particle interactions increase due to the Brownian motion, which is not negligible in these systems. Calculating the rotary particle diffusivity, D_r , assumed to be related to Brownian motion, (Cassagnau 2013; Hong et al. 2008; Letwimolnun et al. 2007; Ren et al. 2003) for rods or nanofibers of length l and diameter d (Cassagnau 2013):

$$D_r = \frac{3K_B T (\ln(\frac{l}{d}) - 0.8)}{\pi \eta_0 l^3} \quad (5)$$

where K_B is the Boltzmann constant ($1.38 \times 10^{-23} \text{ J K}^{-1}$), T is the temperature (443.15 K), η_0 is the polymer viscosity (215 Pa s), D_r is found to be ca. 0.04 s^{-1} . The Brownian motion in absence of flow can play an important role towards the formation of a network and particle–particle interactions. If the rest time is long enough, a network structure is progressively rebuilt, which results in overshoots in the reverse flow. The magnitude of the overshoot in the reverse flow depends on how much the network is restored during rest (Letwimolnun et al. 2007). Letwimolnun et al. (2007) observed a similar behavior

for PP/PP graft maleic anhydride (PP-g-MA)/nanoclay systems.

Structure build-up

Following the discussion in the previous section on microstructure build-up after cessation of a shear flow, this section tackles the effect of the flow history on the evolution of the microstructure in PLA–CNC nanocomposites. The storage modulus, G' , in SAOS experiments as a function of time after the cessation of steady-shear is presented in Fig. 10a for samples pre-sheared at a rate of 5 s^{-1} for 360 s. As expected the neat PLA does not exhibit the formation of any microstructure. However, all PLA–CNC nanocomposites show a structure build-up during the time sweep tests. For each PLA–CNC nanocomposite sample G' grows from an initial value, G'_i , to a time-independent value, G'_∞ . The following empirical exponential relation can be used to describe the data (Khalkhal et al. 2011)

$$G'_t = G'_i + (G'_\infty - G'_i) \left(1 - \exp\left(-\frac{t}{\tau}\right) \right) \quad (6)$$

where τ is the characteristic time of each system representing the rate of structure build-up. A similar relation was used by Mobuchon et al. (2007) for nanoclay (Cloisite 15A) in a blend of two miscible polybutenes. The fits of Eq. 6 for the data of each sample are shown by the dashed lines in Fig. 10. The characteristic time of the samples varies from ca. 647 s for PLA containing 1 wt% CNC to ca. 367 s for the 6 wt% CNC nanocomposite. The decrease in the characteristic time was expected because in a more concentrated sample particle–particle interactions are more pronounced and they can take place soon after cessation of shear flow compared to a less

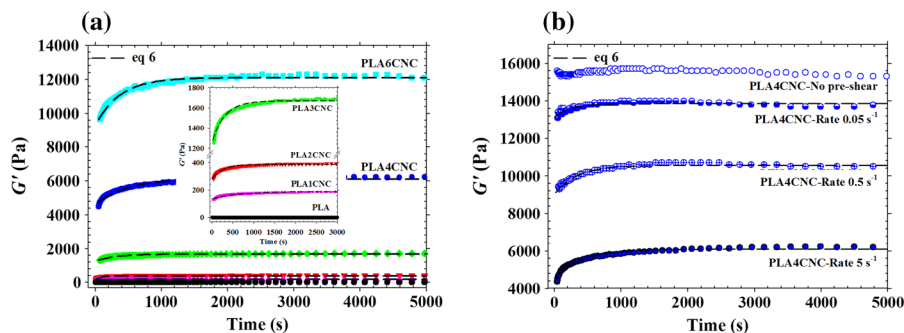


Fig. 10 Structure evolution of PLA–CNC nanocomposites with time right after the cessation of shear flow at $\dot{\gamma} = 5 \text{ s}^{-1}$ (a) (the *inset* shows a magnified part of Fig. 10a); structure development of the PLA4CNC nanocomposite sample not pre-

concentrated sample in which the distances between the particles, after the shear flow, are longer. Besides the effect of concentration on the evolution of the structure after cessation of shear flow, the shear rate at which the samples were pre-sheared can affect the structure build-up. Figure 10b illustrates the development of G' as a function of time after the cessation of flow for different shear rates in PLA containing 4 wt% CNC (PLA4CNC). No build-up in the structure of the sample, which did not experience a shear flow, is exhibited. However, samples that experienced pre-shearing at different rates exhibit a structure build-up with the same trend as observed in Fig. 10a. The larger the pre-shear rate the more destroyed is the initial structure and a larger recovery can be observed after the cessation of shear flow. Using Eq. 6, the characteristic times of the samples were obtained as 273, 340, and 450 s for samples pre-sheared at shear rates of 0.05, 0.5, and 5 s^{-1} , respectively. As expected, the sample sheared at the largest rate (i.e. 5 s^{-1}), requires longer time to build-up its structure due to the more destroyed structure. A value of 600 s was reported as the characteristic time of nanoclay filled system (Mobuchon et al. 2007).

Concluding remarks

In this work for the first time the rheological behavior of the well-dispersed PLA–CNC nanocomposites in SAOS, steady-shear, transient, and structure build-up experiments has been investigated. SEM and TEM images showed that most of the nanoparticles are well

sheared and pre-sheared at $\dot{\gamma}$ of 0.05, 0.5, and 5 s^{-1} (b). G' measured at a frequency of 1 rad s^{-1} and fits using Eq. 6 (dashed lines)

dispersed into the PLA matrix during solution-casting, which favors the wetting of the hydrophilic CNCs within PLA. The addition of CNCs up to 6 wt% resulted in huge increases in the storage modulus and complex viscosity, especially at low frequencies. The rheological percolation threshold was calculated to be as low as 0.68 wt% CNC. Moreover, similar increases in the steady-shear viscosity for all of the nanocomposites were observed. Furthermore, it was found that the PLA–CNC nanocomposites do not obey the Cox–Merz rule. However, for nanocomposites at larger CNC content the extended Cox–Merz rule was applicable. In both SAOS and steady-shear experiments apparent yield stresses were observed for all of the nanocomposites and increased with CNC content. In steady-state experiments, increased viscosity, shear stress, and first normal stress difference were observed and ascribed to the importance of the CNC network and particle–particle interactions. Furthermore, overshoots in shear transient for forward and reverse flows and structure build-up of samples after pre-shearing were ascribed to the network formation. The shear history of the nanocomposite samples was found to affect the behavior of the nanocomposites after cessation of applied shear. The samples pre-sheared at larger rates needed longer time to recover their initial structure. Moreover, structure recovery took place at longer times for less concentrated nanocomposites due to weaker particle–particle interactions.

The rheological properties reported in this work proved the efficiency of the sonicator in solution mixing to disperse the CNCs with the consequent formation of an interconnected network of CNCs

within the PLA matrix. To our knowledge, this is the first time that a very good dispersion of CNCs in a non-hydrosoluble polymer is achieved, without any change in the morphological structure of the CNCs or use of any compatibilizer or modified CNCs.

Acknowledgments The authors acknowledge the financial support from the Natural Sciences and Engineering Research Council of Canada (NSERC). The authors are also grateful to FPIinnovations for providing the CNCs.

References

- Abbasi S, Carreau PJ, Derdouri A, Moan M (2009) Rheological properties and percolation in suspensions of multiwalled carbon nanotubes in polycarbonate. *Rheol Acta* 48:943–959. doi:[10.1007/s00397-009-0375-7](https://doi.org/10.1007/s00397-009-0375-7)
- Abitbol T, Johnstone T, Quinn TM, Gray DG (2011) Reinforcement with cellulose nanocrystals of poly(vinyl alcohol) hydrogels prepared by cyclic freezing and thawing. *Soft Matter* 7:2373–2379. doi:[10.1039/c0sm01172j](https://doi.org/10.1039/c0sm01172j)
- Arias A, Heuzey M-C, Huneault M, Ausias G, Bendahou A (2015) Enhanced dispersion of cellulose nanocrystals in melt-processed polylactide-based nanocomposites. *Cellulose* 22:483–498. doi:[10.1007/s10570-014-0476-z](https://doi.org/10.1007/s10570-014-0476-z)
- Bagheriasl D, Carreau PJ, Dubois C, Riedl B (2015) Properties of polypropylene and polypropylene/poly(ethylene-co-vinyl alcohol) blend/CNC nanocomposites. *Compos Sci Technol* 117:357–363. doi:[10.1016/j.compscitech.2015.07.012](https://doi.org/10.1016/j.compscitech.2015.07.012)
- Bendahou A, Kaddami H, Dufresne A (2010) Investigation on the effect of cellulosic nanoparticles' morphology on the properties of natural rubber based nanocomposites. *Eur Polym J* 46:609–620. doi:[10.1016/j.eurpolymj.2009.12.025](https://doi.org/10.1016/j.eurpolymj.2009.12.025)
- Bitinis N, Verdejo R, Bras J, Fortunati E, Kenny JM, Torre L, Lopez-Manchado MA (2013) Poly(lactic acid)/natural rubber/cellulose nanocrystal bionanocomposites part I. Processing and morphology. *Carbohydr Polym* 96:611–620. doi:[10.1016/j.carbpol.2013.02.068](https://doi.org/10.1016/j.carbpol.2013.02.068)
- Carreau PJ, DeKee DCR, Chhabra RP (1997) Rheology of polymeric systems: principles and applications. Hanser Publications, Munich
- Cassagnau P (2013) Linear viscoelasticity and dynamics of suspensions and molten polymers filled with nanoparticles of different aspect ratios. *Polymer* 54:4762–4775. doi:[10.1016/j.polymer.2013.06.012](https://doi.org/10.1016/j.polymer.2013.06.012)
- Cox WP, Merz EH (1958) Correlation of dynamic and steady flow viscosities. *J Polym Sci* 28:619–622. doi:[10.1002/pol.1958.1202811812](https://doi.org/10.1002/pol.1958.1202811812)
- Doraiswamy D, Mujumdar AN, Tsao I, Beris AN, Danforth SC, Metzner AB (1991) The Cox-Merz rule extended: A rheological model for concentrated suspensions and other materials with a yield stress. *J Rheol* 35:647–685. doi:[10.1122/1.550184](https://doi.org/10.1122/1.550184)
- Du F, Scogna RC, Zhou W, Brand S, Fischer JE, Winey KI (2004) Nanotube networks in polymer nanocomposites: rheology and electrical conductivity. *Macromolecules* 37:9048–9055. doi:[10.1021/ma049164g](https://doi.org/10.1021/ma049164g)
- Favier V, Chanzy H, Cavaille JY (1995) Polymer nanocomposites reinforced by cellulose whiskers. *Macromolecules* 28:6365–6367. doi:[10.1021/ma00122a053](https://doi.org/10.1021/ma00122a053)
- Ghanbari A, Heuzey M-C, Carreau P, Ton-That M-T (2013) Morphological and rheological properties of PET/clay nanocomposites. *Rheol Acta* 52:59–74. doi:[10.1007/s00397-012-0667-1](https://doi.org/10.1007/s00397-012-0667-1)
- Goffin AL, Raquez JM, Duquesne E, Siqueira G, Habibi Y, Dufresne A, Dubois P (2011a) From interfacial ring-opening polymerization to melt processing of cellulose nanowhiskered poly(lactide)-based nanocomposites. *Biomacromolecules* 12:2456–2465. doi:[10.1021/bm200581h](https://doi.org/10.1021/bm200581h)
- Goffin AL, Raquez JM, Duquesne E, Siqueira G, Habibi Y, Dufresne A, Dubois P (2011b) Poly(ϵ -caprolactone) based nanocomposites reinforced by surface-grafted cellulose nanowhiskers via extrusion processing: morphology, rheology, and thermo-mechanical properties. *Polymer* 52:1532–1538. doi:[10.1016/j.polymer.2011.02.004](https://doi.org/10.1016/j.polymer.2011.02.004)
- Hamad WY, Hu TQ (2010) Structure-process-yield interrelations in nanocrystalline cellulose extraction. *Can J Chem Eng* 88:392–402. doi:[10.1002/cjce.20298](https://doi.org/10.1002/cjce.20298)
- Hong JS, Kim YK, Ahn KH, Lee SJ (2008) Shear-induced migration of nanoclay during morphology evolution of PBT/PS blend. *J Appl Polym Sci* 108:565–575. doi:[10.1002/app.27330](https://doi.org/10.1002/app.27330)
- Hu G, Zhao C, Zhang S, Yang M, Wang Z (2006) Low percolation thresholds of electrical conductivity and rheology in poly(ethylene terephthalate) through the networks of multi-walled carbon nanotubes. *Polymer* 47:480–488. doi:[10.1016/j.polymer.2005.11.028](https://doi.org/10.1016/j.polymer.2005.11.028)
- Kamal MR, Khoshkava V (2015) Effect of cellulose nanocrystals (CNC) on rheological and mechanical properties and crystallization behavior of PLA/CNC nanocomposites. *Carbohydr Polym* 123:105–114. doi:[10.1016/j.carbpol.2015.01.012](https://doi.org/10.1016/j.carbpol.2015.01.012)
- Khalkhal F, Carreau PJ, Ausias G (2011) Effect of flow history on linear viscoelastic properties and the evolution of the structure of multiwalled carbon nanotube suspensions in an epoxy. *J Rheol* 55:153–175. doi:[10.1122/1.3523628](https://doi.org/10.1122/1.3523628)
- Khoshkava V, Kamal MR (2014) Effect of cellulose nanocrystals (CNC) particle morphology on dispersion and rheological and mechanical properties of polypropylene/CNC nanocomposites. *ACS Appl Mater Interfaces* 6:8146–8157. doi:[10.1021/am500577e](https://doi.org/10.1021/am500577e)
- Klemm D, Heublein B, Fink HP, Bohn A (2005) Cellulose: fascinating biopolymer and sustainable raw material. *Angew Chem* 44:3358–3393. doi:[10.1002/anie.200460587](https://doi.org/10.1002/anie.200460587)
- Klemm D, Kramer F, Moritz S, Lindstrom T, Ankerfors M, Gray D, Dorris A (2011) Nanocelluloses: a new family of nature-based materials. *Angew Chem* 50:5438–5466. doi:[10.1002/anie.201001273](https://doi.org/10.1002/anie.201001273)
- Letwimolnun W, Vergnes B, Ausias G, Carreau PJ (2007) Stress overshoots of organoclay nanocomposites in transient shear flow. *J Nonnewton Fluid Mech* 141:167–179. doi:[10.1016/j.jnnfm.2006.11.003](https://doi.org/10.1016/j.jnnfm.2006.11.003)
- Mabrouk AB, Magnin A, Belgacem MN, Boufi S (2011) Melt rheology of nanocomposites based on acrylic copolymer and cellulose whiskers. *Compos Sci Technol* 71:818–827. doi:[10.1016/j.compscitech.2011.01.012](https://doi.org/10.1016/j.compscitech.2011.01.012)

- Mobuchon C, Carreau PJ, Heuzey M-C (2007) Effect of flow history on the structure of a non-polar polymer/clay nanocomposite model system. *Rheol Acta* 46:1045–1056. doi:[10.1007/s00397-007-0188-5](https://doi.org/10.1007/s00397-007-0188-5)
- Morandi G, Heath L, Thielemans W (2009) Cellulose nanocrystals grafted with polystyrene chains through surface-initiated atom transfer radical polymerization (SI-ATRP). *Langmuir ACS J Surf Colloids* 25:8280–8286. doi:[10.1021/la900452a](https://doi.org/10.1021/la900452a)
- Natale G, Heuzey MC, Carreau PJ, Ausias G, Férec J (2014) Rheological modeling of carbon nanotube suspensions with rod–rod interactions. *AIChE J* 60:1476–1487. doi:[10.1002/aic.14316](https://doi.org/10.1002/aic.14316)
- Park W-I, Kang M, Kim H-S, Jin H-J (2007) Electrospinning of poly(ethylene oxide) with bacterial cellulose whiskers. *Macromol Symp* 249–250:289–294. doi:[10.1002/masy.200750347](https://doi.org/10.1002/masy.200750347)
- Pereda M, Kissi NE, Dufresne A (2014) Extrusion of polysaccharide nanocrystal reinforced polymer nanocomposites through compatibilization with poly(ethylene oxide). *ACS Appl Mater Interfaces* 6:9365–9375. doi:[10.1021/am501755p](https://doi.org/10.1021/am501755p)
- Peresin MS, Habibi Y, Zoppe JO, Pawlak JJ, Rojas OJ (2010) Nanofiber composites of polyvinyl alcohol and cellulose nanocrystals: manufacture and characterization. *Biomacromolecules* 11:674–681. doi:[10.1021/bm901254n](https://doi.org/10.1021/bm901254n)
- Raquez JM, Murena Y, Goffin AL, Habibi Y, Ruelle B, DeBuyl F, Dubois P (2012) Surface-modification of cellulose nanowhiskers and their use as nanoreinforcers into polylactide: a sustainably-integrated approach. *Compos Sci Technol* 72:544–549. doi:[10.1016/j.compscitech.2011.11.017](https://doi.org/10.1016/j.compscitech.2011.11.017)
- Ren J, Casanueva BF, Mitchell CA, Krishnamoorti R (2003) Disorientation kinetics of aligned polymer layered silicate nanocomposites. *Macromolecules* 36:4188–4194. doi:[10.1021/ma025703a](https://doi.org/10.1021/ma025703a)
- Sepehr M, Ausias G, Carreau PJ (2004) Rheological properties of short fiber filled polypropylene in transient shear flow. *J Nonnewton Fluid Mech* 123:19–32. doi:[10.1016/j.jnnfm.2004.06.005](https://doi.org/10.1016/j.jnnfm.2004.06.005)
- Shafiei-Sabet S, Hamad WY, Hatzikiriakos SG (2012) Rheology of nanocrystalline cellulose aqueous suspensions. *Langmuir ACS J Surf Colloids* 28:17124–17133. doi:[10.1021/la303380v](https://doi.org/10.1021/la303380v)
- Sinha Ray S, Yamada K, Okamoto M, Ueda K (2003) New polylactide-layered silicate nanocomposites. 2. Concurrent improvements of material properties, biodegradability and melt rheology. *Polymer* 44:857–866. doi:[10.1016/S0032-3861\(02\)00818-2](https://doi.org/10.1016/S0032-3861(02)00818-2)
- Siqueira G, Bras J, Dufresne A (2009) Cellulose whiskers versus microfibrils: influence of the Nature of the nanoparticle and its surface functionalization on the thermal and mechanical properties of nanocomposites. *Biomacromolecules* 10:425–432. doi:[10.1021/bm801193d](https://doi.org/10.1021/bm801193d)
- Siqueira G, Abdillahi H, Bras J, Dufresne A (2010) High reinforcing capability cellulose nanocrystals extracted from *Syngonanthus nitens* (*Capim Dourado*). *Cellulose* 17:289–298. doi:[10.1007/s10570-009-9384-z](https://doi.org/10.1007/s10570-009-9384-z)
- Siqueira G, Bras J, Follain N, Belbekhouche S, Marais S, Dufresne A (2013) Thermal and mechanical properties of bio-nanocomposites reinforced by *Luffa cylindrica* cellulose nanocrystals. *Carbohydr Polym* 91:711–717. doi:[10.1016/j.carbpol.2012.08.057](https://doi.org/10.1016/j.carbpol.2012.08.057)
- Zhang W, He X, Li C, Zhang X, Lu C, Zhang X, Deng Y (2014) High performance poly (vinyl alcohol)/cellulose nanocrystals nanocomposites manufactured by injection molding. *Cellulose* 21:485–494. doi:[10.1007/s10570-013-0141-y](https://doi.org/10.1007/s10570-013-0141-y)